Measurement setup for Nernst and Seebeck effect at high temperatures and magnetic fields tested on elemental Bismuth and full-Heusler compounds

M. Parzer,[1, a)] T. Schmid,[1, b)] F. Garmroudi, A. Riss,[1] T. Mori,[2, 3] and E. Bauer[1]
[1)] *Institute of Solid State Physics, Technische Universität Wien, 1040 Vienna, Austria*
[2)] *International Center for Materials Nanoarchitectonics (WPI-MANA), National Institute for Materials Science (NIMS), Tsukuba, Japan*
[3)] *Graduate School of Pure and Applied Science, University of Tsukuba, Tsukuba, Japan*

In this work, a measurement setup to study the Seebeck and Nernst effect at high temperatures and high magnetic fields is introduced and discussed. The measurement system allows for simultaneous measurements of both thermoelectric effects up to 700 K and magnetic fields up to 12 T. Based on theoretical concepts, measurement equations are derived, that counteract constant spurious offset voltages and and therefore inhibit systematic errors of the measurement setup. The functionality is demonstrated on polycrystalline samples of elemental bismuth as well as various full-Heusler materials, exhibiting an anomalous Nernst effect. In all samples, the measured Seebeck and Nernst coefficient aligns excellently with reported values. This allows for future research to substantially extend the measured temperature and field intervals, which are commonly limited to temperatures below room temperature. For the first time, the thermoelectric and thermomagnetic properties of these materials are reported up to temperatures of 560 K.

Introduction

Research on thermoelectric effects constitutes a broad field of physical sciences today, with topics reaching from fundamental studies up to functional prototypes and commercialization of thermoelectric devices.[1–3] For years, most of the application-based research has been focused on the longitudinal thermoelectric effect, namely the Seebeck effect.[4] Only in the last few decades, significant effort has been made towards the application of transverse voltage generation, which can be achieved for example via the Nernst effect.[5] Similar to the well-known Hall effect, an electrical voltage emerges perpendicular to the perpetrating current, if a magnetic field is applied. This is caused by the deflection of the charge carriers by the Lorentz force. The Nernst effect has only recently gained a lot of attention due to the discovery of *giant* anomalous Nernst signals in topological materials.[6–8] For most of these cases the large signal stems from a non-trivial band structure, involving topological bands close to the Fermi level E_F and originates from the resulting Berry curvature. Moreover, the anomalous contribution can be large even at elevated temperatures above $T = 300$ K, bringing this effect closer to possible applications. A recent study by Uchida and Heremans outlined several advantages of energy harvesting based on transverse voltages compared to the Seebeck effect.[9] To explore promising materials for application, but also for fundamental research, reliable and precise measurements of thermoelectric effects are indispensable. While building an experimental setup for Seebeck measurements is simple and compact devices are commercially available, measuring the Nernst effect is more challenging. This is mainly due to lower voltage signals and the requirement of a controllable magnet that can reach reasonably high magnetic fields. Hence, there are significantly less Nernst measurement data published than for the Seebeck coefficient. For temperatures above 400 K there are, to the

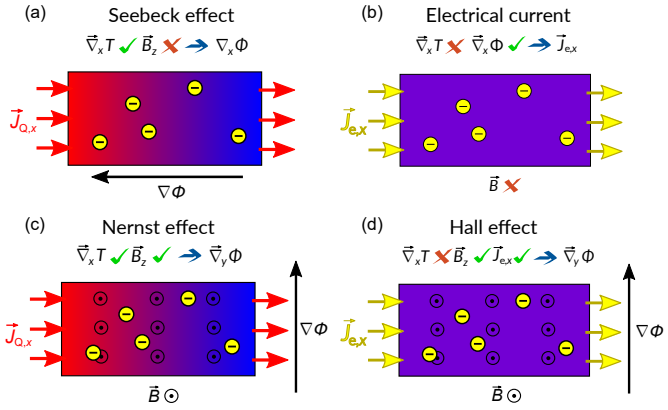

Figure 1: **(Thermo)electric effects** Schematic of the underlying currents and gradients of the four different effects: a) Seebeck effect: A gradient in the electrical potential arising from a temperature gradient; b) Voltage-driven electrical current: The motion of electrons due to a potential gradient in the absence of a temperature gradient c) Nernst effect: Perpendicular voltage gradient arising in the presence of a magnetic field and a temperature gradient orthogonal to each other. d) Hall effect: Perpendicular voltage arising in the presence of a magnetic field and an electrical current normal to each other.

[a)] Electronic mail: michael.parzer@tuwien.ac.at
[b)] Electronic mail: ts.schmid94@gmail.com

best of our knowledge, no published Nernst data so far. This work documents the process of building, optimizing and validating a custom-built measurement setup that can perform simultaneous Seebeck and Nernst effect measurements at high temperatures and high magnetic fields up to 12 T. Additionally, the theory of both effects is discussed, the underlying measurement framework is elucidated and the underlying measurement principles for high temperature measurements and noise reduction are derived. To confirm full functionality of the setup, polycrystalline samples of constantan, bismuth and multiple full-Heusler compounds were synthesized, measured and analyzed. The data are presented and compared with literature data and reference measurements in the results section.

I. Thermoelectric transport

The electrical current in a given material is defined by the two conductivity tensors $\hat{\sigma}$ and $\hat{\alpha}$, the electrical field $\vec{E}$ and the temperature gradient $\vec{\nabla}T$:

$$\vec{J_e} = \hat{\sigma} \cdot \vec{E} - \hat{\alpha}\vec{\nabla}T. \tag{1}$$

In open circuit conditions, hence $J_e = 0$, the equation simplifies to an expression for the electrical field $\vec{E}$:

$$\vec{E} = \hat{\sigma}^{-1} \cdot \hat{\alpha} \cdot \vec{\nabla}T. \tag{2}$$

In other words, an electrical field in a material can be caused by a temperature gradient and is proportional to the ratio of the thermoelectric conductivity to the electrical conductivity. It is a materials property closely connected to the electronic structure and can be derived from Boltzmann theory to[10]

$$\hat{\sigma}^{-1}\hat{\alpha} = -\frac{\pi^2 k_B^2 T}{3e}\hat{\sigma}^{-1}\left(\frac{\partial\hat{\sigma}(E)}{\partial E}\right)|_{E=E_F}. \tag{3}$$

Its magnitude is given by the change of the conductivity at the Fermi energy E_F for infinitesimal shifts of the chemical potential divided by the total electrical conductivity.

Seebeck coefficient

Coming back to Equation 2, only considering a temperature gradient in the x-direction, the field in the x-direction yields:

$$E_x = \alpha_{xx}/\sigma_{xx}\nabla_x T. \tag{4}$$

This proportionality factor regarding the electrical field E_x is denoted as Seebeck coefficient $S = \sigma_{xx}^{-1}\alpha_{xx}$. For small temperature difference ΔT between the contacts, so that $S(T_\mathrm{max}) \approx S(T_\mathrm{min})$, the voltage signal originating from the Seebeck coefficient is given by

$$U_x = S_{xx}\Delta T, \tag{5}$$

and is independent of any dimensions, as long as the voltage is measured at the same position as the temperature gradient.

Nernst effect

Similar considerations can be made for the electrical field in the y-direction E_y. Again, setting the temperature gradient $\nabla_x T$ and demanding $J_{e,x}, J_{e,y} = 0$, a result for the Nernst signal e_N in dependence of $\nabla_x T$ can be derived:

$$e_N = E_y/\nabla_x T = \frac{\alpha_{xy}\sigma_{xx} - \sigma_{xx}\alpha_{xy}}{\sigma_{xx}^2 + \sigma_{xy}^2}. \tag{6}$$

Using the Hall angle $\tan(\theta_H) = \sigma_{xy}/\sigma_{xx}$, Equation 6 can be expressed in a more illustrative way:[11]

$$e_N = \alpha_{xy}/\sigma_{xx} + S \cdot \tan(\theta_H). \tag{7}$$

Thus, two terms can lead to a finite transverse voltage signal e_N caused by a temperature gradient in x. One is proportional to the Seebeck coefficient and the Hall-angle, i.e. the ratio of transverse and lateral electrical conductivity, while the other one is directly proportional to the off-diagonal matrix element of the thermoelectric conductivity tensor α_{xy}. In isotropic materials the off-diagonal elements of both tensors, $\hat{\alpha}$ and $\hat{\sigma}$ are generally zero. When applying a magnetic field H_z, however, the Lorentz force leads to deviation of the charge carriers, leading to finite values for α_{xy} and σ_{xy}, hence to a finite voltage signal $e_N \neq 0$. Consequently, a temperature difference in x-direction leads to a thermovoltage e_N perpendicular to it. A sketch illustrating the various electric and thermoelectric effects is provided in Figure 1. The proportionality constant in y-direction $N = e_N/B$ is denoted as Nernst coefficient. On the contrary, the Nernst signal $e_N = N \cdot B$ is proportional to the magnetic flux density B and can be derived from Boltzmann transport for one band to[10]

$$e_N = -B\frac{\pi^2}{3}\frac{k_\mathrm{B}^2 T}{m^*}\frac{\partial\tau}{\partial E}|_{E=E_\mathrm{F}}, \tag{8}$$

depending on the effective mass m^* and the energy derivative of the scattering time τ at E_F. The measurement equation for the Nernst signal in the y-direction originating from a temperature gradient in the x-direction and a given magnetic field in z-direction can be written as:

$$U_y = N H_z \Delta T_x \frac{\Delta y}{\Delta x}, \tag{9}$$

with the distances between the Nernst contacts Δy and between the Seebeck contacts Δx. Since for magnetic materials $B = \mu_0 H + \mu_0 M$, the Nernst signal can further be split into two components[12]

$$e_N = \mu_0 H_z Q_\mathrm{o} + \mu_0 M_z Q_\mathrm{a}, \tag{10}$$

where μ_0 is the vacuum permeability, M is the magnetization and Q_o, Q_a are the proportionality factors for the ordinary and the anomalous Nernst signals, respectively. Hence, the term anomalous Nernst signal encompasses all effects that scale with the magnetization M.

II. Measurement equations

To analyze the dynamic voltage signals associated with the Seebeck and Nernst effects obtained using the measurement setup described here, we can modify Equations (5, 9). This involves introducing mathematical models and optimizations to eliminate parasitic signals. In the following, the measurement setup and the measured voltages will be illustrated with the help of the sketch of the model setup depicted in Figure 2. As can be seen in Figure 2, there are in total five electrical contacts to the sample. Two R-type thermocouples are used to measure the Seebeck coefficient and temperature gradient at the bottom of the sample in the x-direction. Three copper wires are contacted onto the top of the sample for the measurement of the parallel voltage gradient as well as the voltage in the y-direction. The measurements are conducted using two dual-channel Keithley 2182A nanovoltmeters which can accurately measure two different voltage signals each, if used in one electrical circuit. The external magnetic field is applied in the z-direction while a temperature gradient can be applied along the x-direction

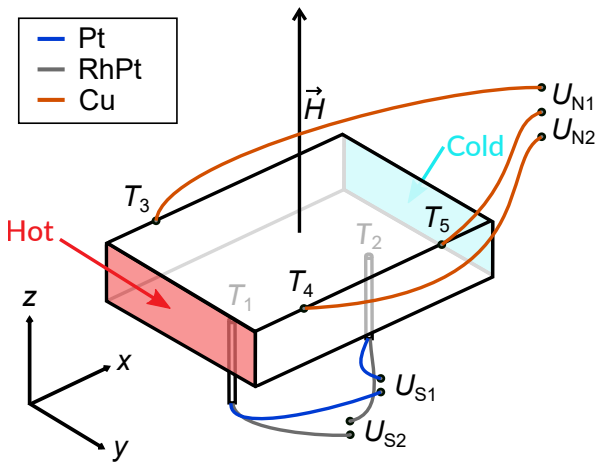

Figure 2: **Model setup for simultaneous Nernst- and Seebeck measurements** The sample is connected to two R-type thermocouples at the bottom and three copper wires are contacted on the top. The voltages are measured using two two-channel nanovoltmeters and are denoted as $U_{N1}, U_{N2}, U_{S1}, U_{N2}$. Each wire's contact point with the sample can be assigned an individual temperature T_1, T_2, T_3, T_4, and T_5. The magnetic field is applied in z-direction while a temperature gradient is created along the x-direction, indicated by the red and blue surfaces.

of the sample. Test measurements have shown that possible spurious temperature gradients in the y-direction are negligible compared to the temperature gradient in x-direction resulting in $T_3 \approx T_4$ and $T_5 - T_4 >> T_4 - T_3$. Using Equations (5, 9), we can explicitly write down the voltages U_{S1}, U_{S2}, U_{N1} and U_{S2} measured by each channel of the sketched contacts for a given temperature gradient $\nabla_x T$ and magnetic field H_z. Again, Δx and Δy denote the distances between the voltage contacts for the Seebeck coefficient (distance between T_5 and T_4) and the Nernst contacts (distance between T_4 and T_3)

$$U_{S1} = (S_X - S_{Pt})(T_2 - T_1), \quad (11)$$

$$U_{S2} = (S_X - S_{RhPt})(T_2 - T_1), \quad (12)$$

$$U_{N1} = (S_X - S_{Cu})(T_5 - T_4) + NH_z \frac{\Delta y}{\Delta x}(T_5 - T_4), \quad (13)$$

$$U_{N2} = (S_X - S_{Cu})(T_5 - T_4). \quad (14)$$

U_{S1} and U_{S2} are the Seebeck voltage measured over the Pt wires and the PtRh%13 wires respectively.

Measuring the Seebeck coefficient

In this configuration, the sample Seebeck coefficient S_X, measured using the thermocouple, can be derived as:

$$S_X = S_{RhPt} - \frac{S_{RhPt} - S_{Pt}}{1 - \frac{U_{S1}}{U_{S2}}}, \quad (15)$$

with S_A, S_B being the Seebeck coefficient of the respective thermocouple wires and U_{S1}/U_{S2} being the ratio of the measured voltages.

Measuring the Nernst coefficient

A similar equation can also be derived for the measurement of the Nernst coefficient:

$$\frac{U_{N1}}{U_{N2}} = 1 + \frac{\Delta y}{\Delta x}\left(\frac{NH_z}{S_{Cu} - S_X}\right). \quad (16)$$

Possible systematic measurement errors from non-parallel contacts can then be eliminated by comparing Equation 16 for two measurements at different values of H_z. By choosing $H_z = 0$ for one of them, which corresponds to a reference measurement without magnetic field, the equation is changed to:

$$\frac{U_{N1}}{U_{N2}}(H_z) - \frac{U_{N1}}{U_{N2}}(0) = \frac{\Delta y}{\Delta x}\left(\frac{NH_z}{S_{Cu}(H_z) - S_X(H_z)}\right). \quad (17)$$

Solving for N yields:

$$N = \frac{\Delta x}{\Delta y}\left(\frac{S_{Cu}(H_z) - S_X(H_z)}{H_z}\right)\left(\frac{U_{N1}}{U_{N2}}(H_z) - \frac{U_{N1}}{U_{N2}}(0)\right). \quad (18)$$

$S_X(H_z)$ is calculated by using Equation 15 in presence of a magnetic field H_z, while $S_{Cu}(H_z)$ is calculated by

using a fit of experimental data for 70 K< T < 1500 K reported in Ref.[13], under the reasonable assumption that its dependence on magnetic field is negligible, $S_{\mathrm{Cu}}(H_z) \approx S_{\mathrm{Cu}}(0)$.

Elimination of spurious offset voltages

In real conditions, Equation 16 and Equation 18 tend to be error-prone when applied to singular measurements, resulting in measurement errors due to spurious offset voltages that can affect each measured signal differently and independently. These spurious voltages likely stem from temperature differences at any electrical connection between different materials or from atmospheric noise along the connectors and can usually not be completely avoided at elevated temperatures.[14] To eliminate the effect of spurious offset voltages, U_{S1} and U_{S2} are measured at multiple temperature gradients. This way, the slope of $\partial U_i/\partial \Delta T$ is obtained, which is independent of any offsets. Ultimately this allows to express Equation 15 as:

$$S_X = S_{RhPt} - \frac{S_{RhPt} - S_{Pt}}{1 - \frac{\partial U_{S1}}{\partial U_{S2}}} \tag{19}$$

This transition mathematically eradicates systematic errors caused by offset voltages of any source as long as they remain constant during each measurement and is especially important for measurements at high temperatures.[15–18]

Similar considerations can be made for the measurement of the Nernst coefficient. Proceeding from Equation 18, it is again possible to replace the ratios of U_{N1} and U_{N2} with their respective derivatives, yielding the following improved measurement equation for the Nernst effect:

$$N = \frac{\Delta x}{\Delta y}\left(\frac{S_{\mathrm{Cu}}(H_z) - S_X(H_z)}{H_z}\right)\left(\frac{\partial U_{N1}}{\partial U_{N2}}(H_z) - \frac{\partial U_{N1}}{\partial U_{N2}}(0)\right). \tag{20}$$

With these equations, a dynamic measurement method for the simultaneous measurement of N and S can be realized to measure the quantities not only faster but especially more accurate than with conventional steady-state measurement methods.

III. Experimental setup

To measure the Nernst and Seebeck effects of a given material above room temperature and high fields, the measurement setup must meet the following requirements:

i) High-field (superconducting) magnet for consistent high magnetic fields as regular electromagnets can only reach fields up to $1.6 - 2\,\mathrm{T}$.[19]

ii) Stable, variable temperature control and control of temperature gradients and high-temperature resistance

iii) Reliable and accurate measurements of the temperature, voltages and temperature gradients

To accomplish those preconditions, extraordinary temperature isolation of the sample space from the superconducting coil must be assured. To keep the coil in its superconducting state below T_c, a reliable cooling system is needed. Our experiment is designed in a way to fulfill these requirements, while still allowing for a simple measurement routine and relatively easy exchange of the sample holder and the samples. A photo, as well as a 2D-sketch of the cut of our measurement setup are presented in Figure 3 a, b.

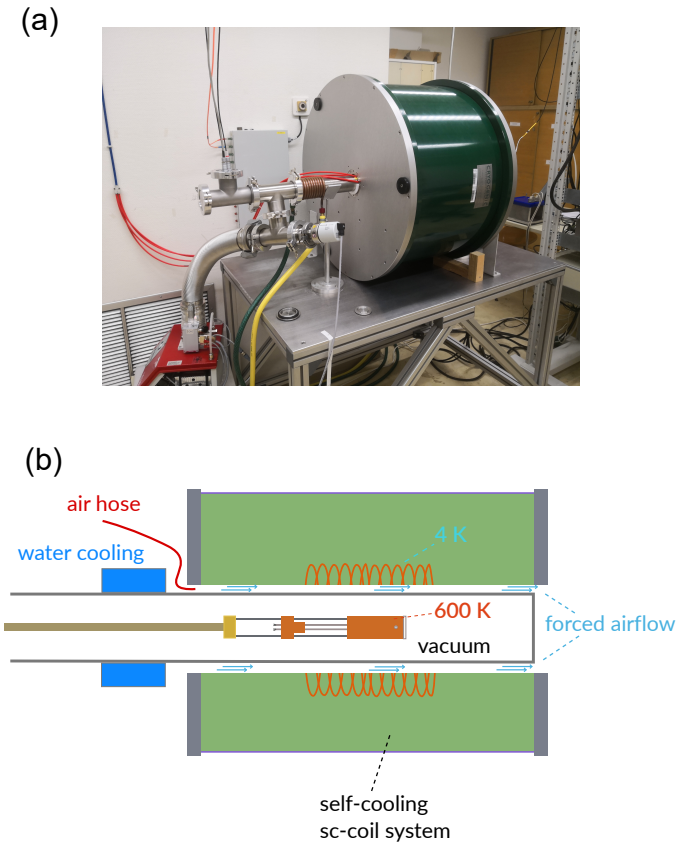

Figure 3: **Experimental setup** a) Image of the experimental setup and b) sketch of the longitudinal section of the same. The high temperature difference between the superconducting coil (4 K) and the sample holder (up to 700 K) is achieved by a high vacuum of up to 10^{-6} mbar in the sample space, extrinsic water cooling of the sample space and forced airflow at the boundary.

Measurement environment

The large magnetic field is achieved using a commercially available ^{4}He refrigeration system from *Cryogenics Ltd* containing a superconducting Nb-Ti coil that can reach fields up to 12 T. The setup has a 65 mm hole that is accessible from the outside and can be readily used. The homogeneity of the magnetic field was tested using nuclear magnetic resonance on ^{63}Cu and is above 99.5 % of the set value around the center 0 ± 1.5 cm. To reach high temperatures inside the coil, without warming it up above its critical temperature $T_c \approx 9.5$ K, we employ high vacuum to the sample chamber down to 10^{-6} mbar and fixed the chamber so that an air gap remains between the chamber and the cryostat. Moreover, thermal decoupling is further facilitated by water cooling at the ends of the sample chamber combined with forced air-flow through the space between the sample chamber and the surrounding cryostat containing the coil.

Sample holder

As sketched in Figure 3 b, the measurement setup insert is designed as a rod that can be inserted into the sample chamber surrounded by the superconducting coil. To reduce thermal conductivity from the connectors and wires, the sample rod has a total length of around 1.2 m and the connection to the sample holder is made with four thin steel studding, with a diameter of 2 mm. The rod is a hollow cylinder made of brass and the signal wires are managed inside the rod to give additional shielding and mechanical stability. A schematic of the upper part of the sample holder is depicted in Figure 4. Its core is a solid copper block, accommodating the sensors and heaters, the thermocouples as well as the sample. It assures good heat anchoring of all parts, as elemental copper features a very high thermal conductivity of up to $\kappa_{\mathrm{Cu}} = 400\,\mathrm{W/mK}$ above room temperature.[20] The base temperature is established with two heating cartridges (1), heated with a maximum output power of 5 W, which are inserted into the copper block. To measure the base temperature, a resistive PT-100 temperature sensor (3) is used, which is inserted into the copper block right below the sample. To facilitate a stable temperature gradient and isolate the sample electrically, it is placed on a Macor plate (7), which is screwed onto the copper block. Macor is an electrically insulating ceramic with a very low thermal conductivity of $\kappa_{\mathrm{Macor}} = 1.5\,\mathrm{W/m{\cdot}K}$.[21] The temperature gradient across the sample is established by locally heating on one side using a high-temperature strain-gauge (6) with a resistance of 120 Ω. On the other end of

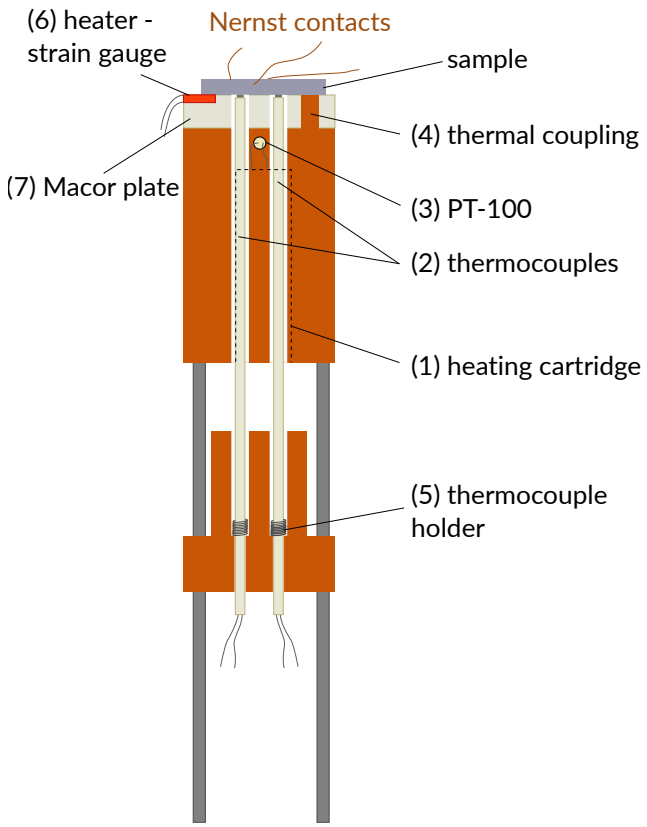

Figure 4: **Sample holder** 2D-sketch of the sample holder at the top of the sample rod. The different components (1-7) are labeled in the figure and described in more detail in the text.

the sample, an extrusion of the copper block (4) is going through the Macor plate, thermally coupling the sample to the base temperature of the copper block, acting as a heat sink. The temperature difference is measured using two R-type thermocouples (2) which are pressed onto the sample by the thermocouple holder (5). They are connected thermally as well as electrically to the sample and the voltages are measured across the wires of the same material (Pt-Pt and Pt13%Rh-Pt13%Rh). This way, the Seebeck coefficient of the sample can directly be obtained using Equation 19. For type-R thermocouples the temperature-dependent Seebeck coefficients of the individual wires (Pt, Pt13%Rh are very well known and reference curves are available.[13,22]. For the measurement of the Nernst coefficient, three copper wires are attached to the sample via spot-welding or silver paste. The wires are placed in a triangular configuration onto the sample as sketched in Figure 2. Two voltages are measured, one parallel to the heat current and one diagonal, including both the longitudinal as well as the transverse signal. As described earlier, a dynamic measurement method is used for the determination of the Seebeck and Nernst coefficients. The base temperature of the whole setup is set via the cartridge heaters. One side of the sample is then heated until a sufficient and stable temperature gradient is reached. As the heater is turned off, the nanovoltmeters measure the signal continuously, determining the voltage signals for a multitude of different temperature gradients. Fitting the slope of the voltage U_{S1} *versus* U_{S2} linearly, gives the correct values of S and N at the respective temperatures, when plugged in the corresponding equation. The dynamic measurement at a certain T and H can be repeated to average of the coefficient and achieve a reduction of the noise. Figure 5 shows a sketch of the time-dependent measurement parameters during a measurement cycle.

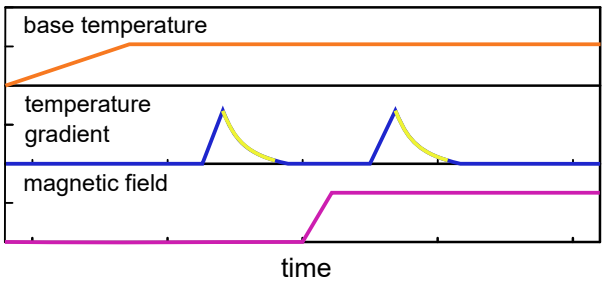

Figure 5: **Sketch of the measurement process** The three graphs show a sketch of the time dependence of the base temperature, the applied temperature difference on the sample and the magnetic field, respectively. The yellow lines in the middle panel represent the time-intervals in which the thermoelectric voltages are measured.

Measurement software

A measurement software including a user interface was designed to control and automate the measurement process introduced above. The communication with the measurement devices is managed via individual socket servers for each device, respectively. The main program is written in Python3 and reads the starting parameters and measurement program from the user input and then controls the whole measurement process. The software is discussed in more detail in Ref.[23], including snapshots of the user interface.

IV. Experimental results

To ensure the functionality of the here-presented measurement setup, different samples were synthesized, measured and compared with available data in literature. Insert discussion of measurement error here All samples presented here were prepared as polycrystalline ingots using high-frequency induction melting. For this process, the samples were weighed in using high-purity bulk elements and a scale with an accuracy of 10 µg and melted with a mass loss below 0.1 %. The samples were confirmed to be single-phase and in the correct crystal structure by X-ray diffraction measurements.

Constantan

The material constantan is most commonly used as reference material for high-temperature Seebeck measurement setups.[13,24–27] Therefore, it was also chosen as reference material for the Seebeck coefficient here because reliable reference data of this material exist. Constantan is the commercial name for a metallic Cu-Ni alloy consisting of roughly 55% Copper and 45% Nickel.[28] It is well-known and named after its constant temperature-dependent resistivity, but also exhibits a sizeable Seebeck coefficient for a metal, due to strong interband scattering.[29] In Figure 6 the comparison of the measurement data for constantan obtained at our lab with reference curves from two different round robin studies is given.[24,25] The measurement data obtained from the newly built setup are in excellent agreement with the reference data as well as with the data from the ZEM-3 measurement on the same sample piece.

Bismuth

Elemental bismuth displays the highest measured value of the absolute Nernst coefficient of all materials and is therefore an optimal candidate for first test measurements.[30] Already in their original publication, Nernst and Ettinghausen noted the extraordinary high Nernst coefficient of Bi compared to other elemental materials such as nickel, cobalt, iron and antimony.[31] It features a semi-metallic electronic density of states with very high-mobility charge carriers and exhibits a relatively high thermoelectric performance and a strong magnetic-field-dependence of the Seebeck coefficient $S(B)$.

Figure 7 a,b shows our measured values of the field-dependent Seebeck and Nernst coefficients of polycrystalline Bi for different temperatures. For comparison, the measurement results from Hamabe *et al.*[32] at 290 K are plotted as grey crosses. As they report the magnetic field dependence of the thermoelectric effects in polycrystalline bismuth up to 290 K, their data can be best compared with our measurement results. Taking into account the temperature dependence of S, N for Bismuth and also the fact that different samples from different labs were measured, very good agreement between the two data sets was found.

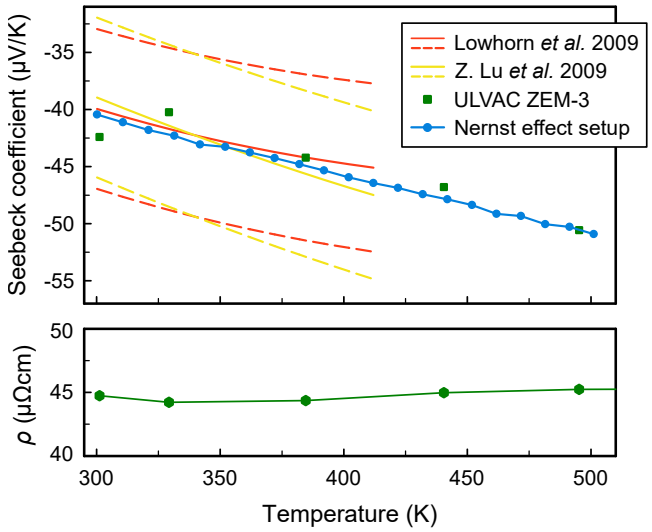

Figure 6: **Seebeck coefficient and resistivity of Constantan** The upper panel shows the measured Seebeck coefficient results of Constantan as function of temperature compared with reference data of Z. Lu *et al.* 2009[24] and N. Lowhorn 2009 *et al.*[25]. The solid lines depict the common curve (expectation value), while the dashed lines visualize the standard deviation derived from the round-robin measurements. The lower panel depicts temperature-dependent resistivity $\rho(T)$ measured with the ULVAC ZEM-3.

Heusler compounds

To verify the capability of the measurement system to measure smaller values of the Nernst coefficient accurately, we studied different full-Heusler compounds, which have been reported to exhibit anomalous Nernst signals.

$Co_2MnAl_{0.63}Si_{0.37}$

Co_2MnZ(Z=Al,Ga) compounds have been predicted to exhibit Weyl points near E_F, expected to give rise to a large anomalous Nernst effect due to the Berry curvature.[33–35] Sakuraba *et al.* experimentally validated that for Co_2MnAl the substitution of Al with Si leads to a shift of the position of the Fermi level E_F and improved $L2_1$ atomic ordering. This leads to a significant enhancement of the anomalous Nernst effect.[35] The highest value of the Nernst signal, 5.7 µV/K at 300 K was reported for 30 nm single crystal films of $Co_2MnAl_{0.63}Si_{0.37}$ annealed at 700 C and measured at room temperature and saturates at around 1 T. As crystalline order is pivotal for the Nernst coefficient in this system, they found a clear correlation between annealing temperature and the magnitude of the Nernst signal e_N. As the crystalline ordering process might occur differently in our bulk samples, the samples were heat-treated at 900 C to ensure good chemical ordering. The polycrystalline bulk sample shows very similar Nernst signals, indicating that the

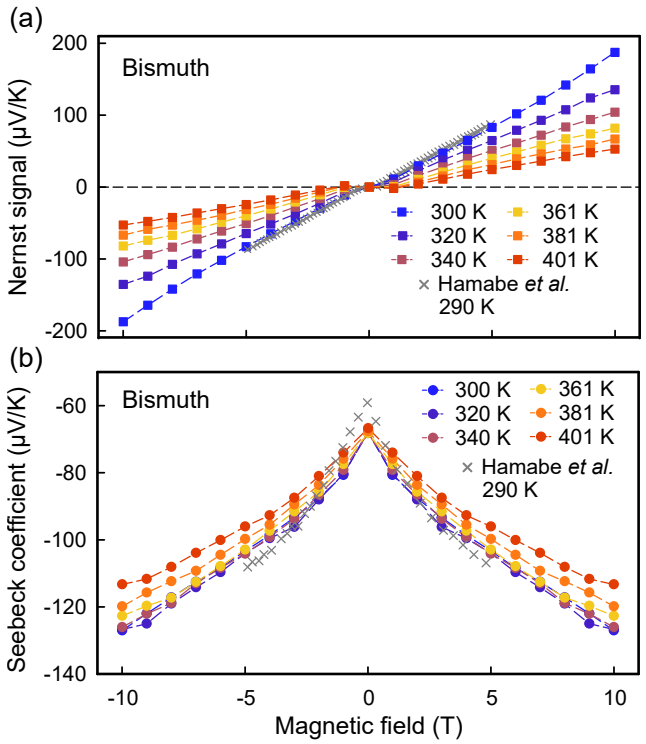

Figure 7: **Measurement results for elemental Bismuth:** The upper panel depicts the measured Nernst signal of Bismuth as a function of magnetic field for different temperatures. Panel b) shows the measurement results for the Seebeck coefficient of Bismuth as a function of magnetic field.

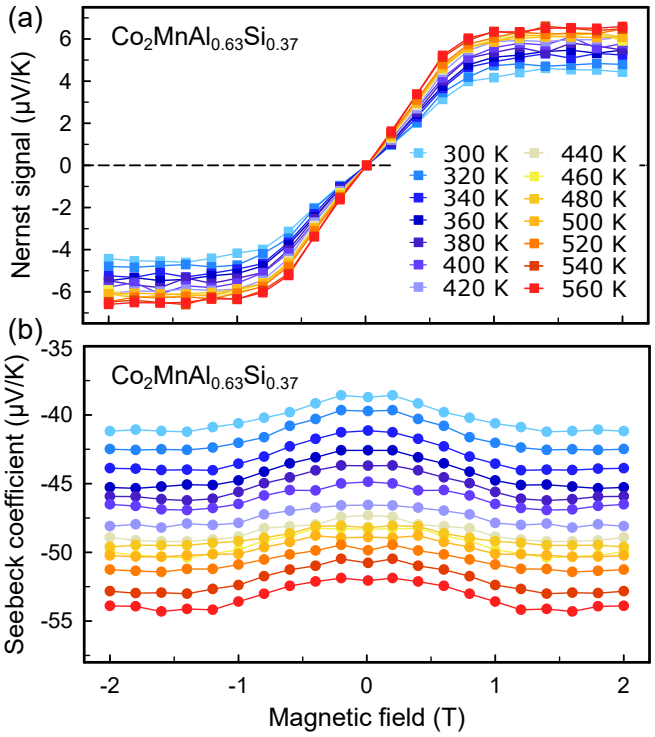

Figure 8: **Measurement results for $Co_2MnAl_{0.63}Si_{0.37}$** Panel a) depicts the field-dependent Nernst effect of of $Co_2MnAl_{0.63}Si_{0.37}$. In panel b) the field-dependent Seebeck coefficient is shown.

higher annealing temperatures had no further effect on the Nernst coefficient. Furthermore, different from literature, the Nernst coefficient of this sample was measured up to 560 K.

Fe_2 based Heusler compounds

An anomalous Nernst effect has also recently been observed for various Fe-based Heusler compounds Fe_2YZ (Y = Co, Ni; Z = Al/Ga)[36]. Similar to $Co_2MnAl_{0.63}Si_{0.37}$, a large intrinsic Berry curvature is responsible for the sizable anomalous Nernst effect in these compounds. Hence, we prepared and measured Fe_2CoAl and Fe_2NiAl for comparison with the published results. Notably, while Mende *et al.* investigated single crystals synthesized via the Bridgeman method[36], our measured values on polycrystalline samples are in excellent agreement with the published results. Compared to $Co_2MnAl_{0.63}Si_{0.37}$, the Nernst coefficients are considerably lower but still a characteristic data-set could be obtained using our measurement setup. For both samples, an increase of $N(T)$ with rising temperature was observed in agreement with the prediction of Mende *et al.*.[36]

Fe_3Z-based compounds

Another recent publication[8] provided detailed theoretical and experimental results for the anomalous Nernst effect of Fe_3Z (Z=Al/Ga).[8] It was shown that the 25 % substitution of aluminum or gallium in α-Fe dramatically increases the anomalous Nernst effect by a factor of more than 10, compared to undoped α-Fe. The reported maximum value of the anomalous Nernst effect of Fe_3Al is around 4 μV/K at room temperature. Data obtained on our bulk Fe_3Al are in good agreement with Ref.[8] but reach the maximum value at higher fields of around 1 T, very similar to the other polycrystalline bulk samples discussed above. To corroborate our results on Fe_3Al, a test measurement of the same sample piece of Fe_3Al was conducted at the CNRS in Paris. The comparison of our measurement results with the data obtained at their low temperature measurement setup is depicted in Figure 10. The measurement setup is designed as inset for a PPMS and is similar to the setup described in the supplemental information of Ref.[37]. Excellent agreement between the measurement data was achieved, regardless of the significant differences in the experimental setup and measurement technique.

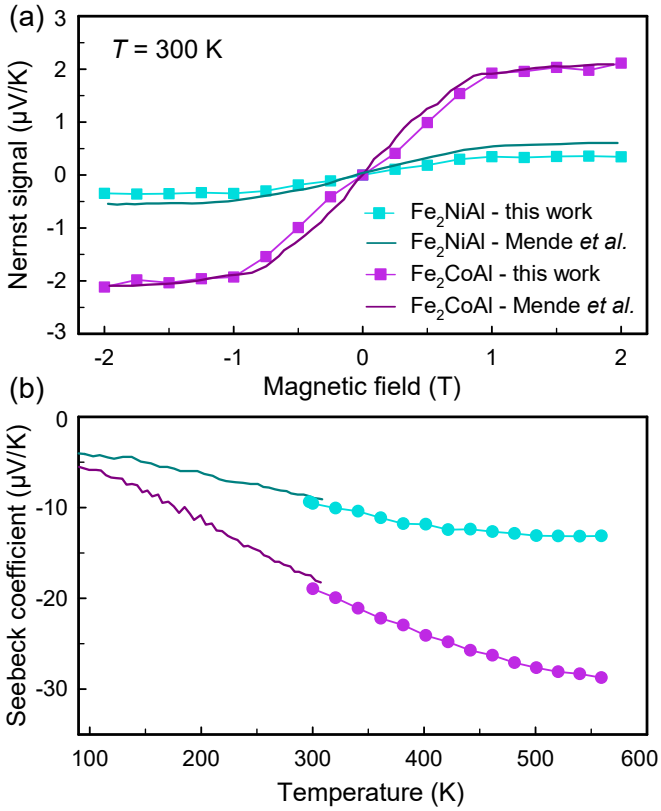

Figure 9: **Measurement results for Fe_2YAl** Measurement data of the Nernst coefficient of Fe-based Heusler alloys compared with available data from the literature.[36] b) Measurement results of the Seebeck coefficient of Fe_2-based Heusler alloys as function of temperature for different values of magnetic field.

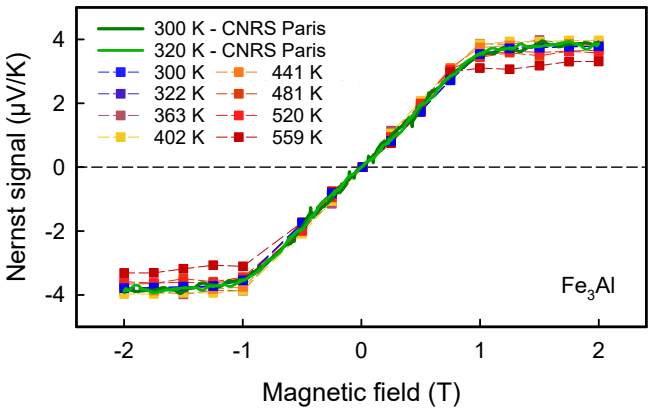

Figure 10: **Measurement results for Fe_3Al** Magnetic field-dependence of the Nernst signal of Fe_3Al for different measurement temperatures between 300-560 K measured with this setup. The measurement at CNRS Paris on the same sample piece at $T = 300, 320$ K is superimposed as green lines for comparison.

V. Conclusion

Summarizing, the two thermoelectric effects, namely the Seebeck and the Nernst effect were discussed and the respective measurement equations were derived. We examined the experimental setting required for the measurement at high fields and temperatures and the implementation thereof in our setup. The measurement setup including the sample chamber, the sample holder and the measurement principle were discussed in detail. To confirm the functionality of the measurement setup, a number of test measurements were conducted on different materials and the data obtained were compared to available data in the literature. For all measured samples, very good agreement between the different data sets was achieved. Notably, our polycrystalline bulk samples show similar Seebeck and Nernst coefficients, compared with the data from single-crystal and thin film studies. Reference measurements with established measurement setups were done on the same sample pieces for constantan and Fe_3Al for the Seebeck and Nernst coefficients, respectively. For both cases, excellent agreement between the data sets was achieved. This nicely demonstrates the functionality and applicability of our system to simultaneously measure magneto-Seebeck and Nernst effects at high temperatures and high fields. It has been tested up to 600 K but the constituting materials can withstand higher temperatures above 700 K. Finally, we want to note that measurement setups like ours, can be easily extended to additionally measure the resistivity and Hall coefficient of the sample at the same time.

Acknowledgment

The research in this paper was supported by the Japan Science and Technology Agency (JST) program MIRAI, No. JPMJMI19A1. We acknowledge X-ray center of the TU Wien for providing the means for the X-ray diffraction measurements and analysis. The authors want to thank H. Müller very much for his help with setting up the experiment as well as as the measurement software. We would like to acknowledge B. Fauqué and K. Behnia from CNRS Paris for generously providing access to their Nernst measurement device used to validate the built-up device in this study and S. Jiang for his help with preparing the sample. We appreciate their commitment to advancing scientific knowledge and their willingness to share resources.

Author contribution

M. Parzer, T. Schmid and E. Bauer conceptualized the work and the experiments. M. Parzer and T. Schmid designed and built up the measurement setup. T. Schmid

derived the optimized measurement equations and implemented them into the setup. T. Schmid and M. Parzer synthesized the samples, did the measurements and wrote the initial draft. M. Parzer, T. Schmid, F. Garmroudi, A. Riss, T. Mori and E. Bauer discussed the results and edited the final manuscript. E. Bauer and T. Mori organized the funding.

Conflict of Interest

The authors have no conflicts to disclose.

Data Availability

The data that support the findings of this study are available from the corresponding author upon reasonable request.

References

[1] V. Pecunia, S. R. P. Silva, J. D. Phillips, E. Artegiani, A. Romeo, H. Shim, J. Park, J.-H. Kim, J. S. Yun, and G. C. Welch, Journal of Physics: Materials (2023).

[2] D. Zhao and G. Tan, Applied thermal engineering **66**, 15 (2014).

[3] G. J. Snyder, A. Pereyra, and R. Gurunathan, Advanced Functional Materials **32**, 2112772 (2022).

[4] D. Champier, Energy Conversion and Management **140**, 167 (2017).

[5] H. Goldsmid, Journal of electronic materials **40**, 1254 (2011).

[6] K. Manna, Y. Sun, L. Muechler, J. Kübler, and C. Felser, Nature Reviews Materials **3**, 244 (2018).

[7] S. N. Guin, K. Manna, J. Noky, S. J. Watzman, C. Fu, N. Kumar, W. Schnelle, C. Shekhar, Y. Sun, J. Gooth, *et al.*, NPG Asia Materials **11**, 16 (2019).

[8] A. Sakai, S. Minami, T. Koretsune, T. Chen, T. Higo, Y. Wang, T. Nomoto, M. Hirayama, S. Miwa, D. Nishio-Hamane, *et al.*, Nature **581**, 53 (2020).

[9] K.-i. Uchida and J. P. Heremans, Joule **6**, 2240 (2022).

[10] K. Behnia, *Fundamentals of thermoelectricity* (OUP Oxford, 2015).

[11] W.-L. Lee, S. Watauchi, V. Miller, R. Cava, and N. Ong, Physical review letters **93**, 226601 (2004).

[12] K.-i. Uchida, W. Zhou, and Y. Sakuraba, Applied Physics Letters **118** (2021).

[13] A. Guan, H. Wang, H. Jin, W. Chu, Y. Guo, and G. Lu, Review of Scientific Instruments **84**, 043903 (2013), https://doi.org/10.1063/1.4798647.

[14] J. de Boor and E. Müller, Review of Scientific Instruments **84**, 065102 (2013), https://doi.org/10.1063/1.4807697.

[15] S. Iwanaga, E. S. Toberer, A. LaLonde, and G. J. Snyder, Review of Scientific Instruments **82** (2011).

[16] J. de Boor and E. Mueller, Review of scientific instruments **84** (2013).

[17] J. de Boor, C. Stiewe, P. Ziolkowski, T. Dasgupta, G. Karpinski, E. Lenz, F. Edler, and E. Mueller, Journal of electronic materials **42**, 1711 (2013).

[18] K. A. Borup, J. De Boor, H. Wang, F. Drymiotis, F. Gascoin, X. Shi, L. Chen, M. I. Fedorov, E. Müller, B. B. Iversen, *et al.*, Energy & Environmental Science **8**, 423 (2015).

[19] T. A. Short, *Electric power distribution handbook* (CRC press, 2003).

[20] J. G. Hust and A. B. Lankford, *Thermal conductivity of aluminum, copper, iron, and tungsten for temperatures from 1 K to the melting point*, Tech. Rep. (National Bureau of Standards, Boulder, CO (USA). Chemical Engineering . . . , 1984).

[21] Corning - macor data sheet, https://www.corning.com/media/worldwide/csm/documents/71759a443535431395eb34ebead091cb.pdf, accessed: 2023-08-22.

[22] Nist typer thermocouple reference data, https://srdata.nist.gov/its90/download/type_r.tab.

[23] T. Schmid, *Nernst-and Seebeck effect at high temperatures and high magnetic fields*, Master's thesis, Wien (2022).

[24] Z. Lu, N. D. Lowhorn, W. Wong-Ng, W. Zhang, E. L. Thomas, M. Otani, M. L. Green, T. N. Tran, C. Caylor, N. Dilley, *et al.*, Journal of research of the National Institute of Standards and Technology **114**, 37 (2009).

[25] N. Lowhorn, W. Wong-Ng, W. Zhang, Z. Lu, M. Otani, E. Thomas, M. Green, T. Tran, N. Dilley, S. Ghamaty, *et al.*, Applied Physics A **94**, 231 (2009).

[26] J. Martin, W. Wong-Ng, T. Caillat, I. Yonenaga, and M. L. Green, Journal of Applied Physics **115** (2014).

[27] Q. Fu, Y. Xiong, W. Zhang, and D. Xu, Review of Scientific Instruments **88** (2017).

[28] J. R. Davis *et al.*, *Copper and copper alloys* (ASM international, 2001).

[29] R. B. K. M. B. Garmroudi, Parzer and Pustogow, Science advances.

[30] K. Behnia, M.-A. Méasson, and Y. Kopelevich, Physical review letters **98**, 076603 (2007).

[31] W. Nernst, Annalen der Physik **267**, 760 (1887).

[32] M. Hamabe, S. Yamamoto, S. Yamaguchi, H. Takahashi, H. Okumura, I. Yonenaga, T. Sasaki, and K. Watanabe, in *Proceedings ICT'03. 22nd International Conference on Thermoelectrics (IEEE Cat. No. 03TH8726)* (IEEE, 2003) pp. 567–570.

[33] J. Kübler and C. Felser, Europhysics Letters **114**, 47005 (2016).

[34] A. Sakai, Y. P. Mizuta, A. A. Nugroho, R. Sihombing, T. Koretsune, M.-T. Suzuki, N. Takemori, R. Ishii, D. Nishio-Hamane, R. Arita, *et al.*, Nature Physics **14**, 1119 (2018).

[35] Y. Sakuraba, K. Hyodo, A. Sakuma, and S. Mitani, Phys. Rev. B **101**, 134407 (2020).

[36] F. Mende, J. Noky, S. N. Guin, G. H. Fecher, K. Manna, P. Adler, W. Schnelle, Y. Sun, C. Fu, and C. Felser, Advanced Science **8**, 2100782 (2021).

[37] M. Hirschberger, L. Spitz, T. Nomoto, T. Kurumaji, S. Gao, J. Masell, T. Nakajima, A. Kikkawa, Y. Yamasaki, H. Sagayama, *et al.*, Physical Review Letters **125**, 076602 (2020).